Composites Part C: Open Access 18 (2025) 100663

Contents lists available at ScienceDirect

Composites Part C: Open Access

journal homepage: www.elsevier.com/locate/composites-part-c-open-access

Effective properties of viscoelastic piezoelectric materials using homogenisation on representative volume finite elements

Felipe Ruivo Fuga [a], Yunior Muñoz Naranjo [a], Reinaldo Rodríguez-Ramos [b], José Antonio Otero [c], Volnei Tita [d,e,*], Ricardo De Medeiros [a]

[a] Department of Mechanical Engineering, Universidade do Estado de Santa Catarina, Paulo Malchitzki, 200, Joinville, 89219-710, Santa Catarina, Brazil
[b] Facultad de Matemática y Computación, Universidad de La Habana, La Habana, 10400, Cuba
[c] Escuela de Ingeniería y Ciencias Tecnologico de Monterrey, Atizapán de Zaragoza, 52926, Mexico
[d] Faculty of Engineering of University of Porto, Department of Mechanical Engineering, Rua Dr. Roberto Frias s/n, Porto, 4200-465, Portugal
[e] University of São Paulo, São Carlos School of Engineering, Department of Aeronautical Engineering, Av. João Dagnone 1100, São Carlos, 13563-120, São Paulo, Brazil

ARTICLE INFO

Keywords:
Piezoelectricity
Viscoelasticity
Finite element method
Representative volume elements
Asymptotic homogenisation method

ABSTRACT

This paper introduces a comprehensive methodology for determining the effective piezo-electromechanical properties considering viscoelastic effects in the composite material. The methodology uses finite element (FE) analysis and homogenisation. By formulating the FE solution as a dynamic equilibrium problem, the proposed approach effectively couples linear elastic piezoelectric fibres within a linear viscoelastic matrix. This couples both complex constitutive behaviours into a single representative cell for time-dependent quasi-static load cases. A virtual stress relaxation test is conducted on a Representative Volume Element (RVE) with periodic boundary conditions. The methodology disregards inertial effects to represent quasi-static loading conditions. It assumes a polymeric matrix phase with only mechanical degrees of freedom. The computed effective time-dependent constitutive coefficients are compared with analytical solutions derived from effective field and asymptotic homogenisation methods for a circular piezoelectric fibre in a viscoelastic polymeric matrix. Despite the simplifying assumption for the polymer matrix, the usage of a time-independent Halpin–Tsai model for effective electric permittivity, coupled with the proposed FE approach, accurately predicts time-dependent behaviour of elastic, piezoelectric and dielectric effective coefficients for different fibre volume ratios. Thus, the proposed approach provides a robust and versatile framework for characterising effective piezoviscoelastic properties. This makes a contribution to the field of micromechanical piezoelectric simulation, paving the way for future research into dynamic effects, more complex material constitutive models, and intricate geometric features.

1. Introduction

The usage of smart structures with embedded sensors, actuators, and energy harvesting capabilities has been a topic of interest for structural designers, particularly those involved in designs that account for damage tolerance, instability attenuation, and self-powered electrical components. Most commonly, piezoelectric crystals such as lead zirconate titanate (PZT) are embedded on polymeric thermoset or thermoplastic matrices, constituting a composite component [1–3]. Alternatively, cellular polymeric films act as piezoelectric sensors upon deformation of charged voids, being called as piezoelectret [4]. Owing to the viscoelastic constitutive behaviour of polymeric matrices, the effective mechanical, electrical, and piezoelectric characteristics of these sensors are time-dependent, being relevant for the optimal design of structural smart systems. Experimental constitutive characterisation of these piezoelectric components requires not only multiple tests due to the anisotropy introduced by the composite material, but also testing under different strain rates. Thus, testing campaigns often lead to time-consuming and expensive activities. Therefore, analytical and numerical methods are commonly employed to describe the effective homogenised constitutive response of piezoelectric materials at a microscopic scale.

Researchers have extensively investigated the time-dependent characteristics of composite materials. Li et al. [5] studied the creep response of carbon nanotube-reinforced polymer composites, using linear viscoelasticity coupled with the Laplace-Carson transform and the

* Corresponding author at: Faculty of Engineering of University of Porto, Department of Mechanical Engineering, Rua Dr. Roberto Frias s/n, Porto, 4200-465, Portugal.
E-mail address: voltita@fe.up.pt (V. Tita).

https://doi.org/10.1016/j.jcomc.2025.100663
Received 20 August 2025; Received in revised form 14 October 2025; Accepted 16 October 2025
Available online 31 October 2025

Mori–Tanaka method. Extending that approach, Muliana [6] developed a micromechanical model for the time dependency of piezo-composites, incorporating matrix viscoelasticity using a Prony series, where a decreasing trend for the time-dependent piezoelectric constant was achieved as fibre volume ratio increased. Similarly, Li and Zhang [7] applied a Prony series model to fibre-reinforced composites, focusing on matrix viscoelasticity and comparing a semi-analytical model to finite element analysis using Representative Volume Elements (RVEs) and numerical homogenisation results. Zhai et al. [8] developed a time-domain asymptotic homogenisation method to directly compute effective viscoelastic properties, without Laplace transforms, using an integral form of the Kelvin–Voigt model and a single characteristic displacement tensor. The proposed methodology was compared with finite element analysis, showing accurate results for unidirectional and woven composites.

Recent works on viscoelastic composites frequently use unit cell models and homogenisation. Berger et al. [9] and Cruz-González et al. [10] developed unit cell models to compute the effective properties and understand the microscale response of fibrous and three-dimensional viscoelastic composites, respectively. Otero et al. [11] and Rodríguez-Ramos et al. [12] further explored this, applying asymptotic and numerical homogenisation, to determine effective constitutive properties under stress relaxation. In addition, Azrar et al. [13] provided analytical solutions for the frequency and time-dependent electro-mechanical properties of piezoelectric composites. Vogel et al. [14] and Li et al. [15] contributed to understanding viscous electro-active polymers and the viscoelastic effects on soft piezoelectric nanocomposites through both simulation and experimental studies. Otero et al. [16] explored homogenisation for fractional visco-piezoelectric fibrous composites, highlighting ongoing research into complex material laws. These studies collectively provide a solid basis for analytical homogenisation procedures that account for viscoelasticity and piezoelectricity. Within the analytical homogenisation methods, the Halpin–Tsai [17] prediction of the elastic moduli of composite materials [18,19] allows for broader applications on electric and thermal properties characterisation. For instance, McCullough [20] showed how similar rules can predict transport properties such as electrical conductivity, thermal conductivity, dielectric constants, and diffusion coefficients in heterogeneous media. Additionally, studies on porous piezoelectric materials by Martínez-Ayuso et al. [21] and functionally graded graphene-reinforced piezoelectric composites by Adhikari et al. [22] show applications in characterising complex electromechanical behaviour and determining effective properties. These examples highlight the Halpin–Tsai method's robust theoretical basis, making it adaptable for various physical phenomena beyond just elastic behaviour.

Finite Element (FE) homogenisation procedures are widely used to analyse the microscale response of complex piezoelectric and viscoelastic materials based on their microstructural properties. For piezoelectric materials, these methods enable the accurate determination of effective elastic, piezoelectric, and dielectric constants, even for cases with complex geometric features [23]. Malakooti and Sodano [24] demonstrated, via FE homogenisation the effective electric properties of composites containing multiple inclusion phases. Longo et al. [25] recently introduced a combined numerical and analytical methodology for analysing hybrid laminates with multi-oriented piezoelectric and structural layers. Araújo et al. [26] addressed the computation of piezoelectric and viscoelastic properties in thin laminates subjected to free vibration using gradient-based optimisation techniques. Naik et al. [27] applied micromechanical approaches to characterise the viscoelastic behaviour of fibrous composites with various RVE configurations. Bouhala et al. [28] integrated numerical and experimental methods to predict the mechanical properties of carbon fibre woven composite. Multi-scale finite element models, ranging from micro to macro scales, were developed using *TexGen* software for textile RVE generation and Abaqus/*Standard*, accounting for resin voids. Three-point bending tests confirmed strong agreement between simulation and experimental results.

As discussed by Tian et al. [29], the evaluation of effective mechanical properties of composites with complex microstructures requires appropriate periodic boundary conditions to be enforced. Furthermore, the viscoelastic behaviour of components, such as in dielectric elastomers, can be effectively captured through continuum mechanical formulations and their FE implementation, as demonstrated by Bueschel et al. [30]. However, the coupling of linear viscoelasticity and linear piezoelectric material behaviour is usually not enabled within commercial finite element codes. Furthermore, a time-dependent solution scheme is required for the viscoelastic response, thus preventing the usage of conventional linear static numerical solvers. Therefore, the accurate simulation of time-dependent piezoelectricity for smart materials leads to complex, non-linear equilibrium analysis within a FE framework.

This paper proposes a comprehensive methodology for determining the effective piezo-electromechanical properties considering viscoelastic effects in the composite material. The novelty of the work lies in the dynamic equilibrium enforced over the RVE so that both viscoelastic and piezoelectric elements are implemented in a time-dependent solution scheme. Inertial effects were disregarded, and a virtual stress relaxation test was performed, ensuring that viscoelasticity is the only time-dependent behaviour introduced. Periodic boundary conditions were enforced using the node-to-node method [25,29], followed by the post-processing of volume-averaged stress and strains. Effective time-dependent constitutive coefficients were computed throughout time and compared to asymptotic homogenisation analytical methods for a circular piezoelectric fibre in a viscoelastic matrix. The proposed FE-based homogenisation procedure was able to predict time-dependent behaviour for elastic, piezoelectric and dielectric effective coefficients for different fibre volume ratios. This methodology provides a versatile and accurate modelling approach for FE-based homogenisation procedures, while using commercial finite element codes.

2. Methodology

This study addresses the formulation of a finite element framework for modelling a polymer matrix phase with a piezoelectric embedded fibre, as shown in Fig. 1. Therefore, the piezoelectric material microstructure consists of a periodic RVE throughout the domain. This work focuses on such RVE, representative of a square/circular fibre packing, as squares and circles describe the cross-section of the geometry. Commonly used as matrix constituents, epoxy resins display viscoelastic behaviour and small dielectric constants without piezoelectricity effects. Therefore, the proposed model assumes the matrix as a domain with mechanical Degrees of Freedom (DOF) only, coupled with a piezoelectric fibre.

Within a displacement-based FE framework, dynamic equilibrium is evaluated according to the system of equations in Eq. (1) for a piezoelectric domain, as implemented by Araújo et al. [26],

$$\begin{bmatrix} M & 0 \\ 0 & 0 \end{bmatrix} \begin{Bmatrix} \{\ddot{u}\}(t) \\ \ddot{\phi}(t) \end{Bmatrix} + \begin{Bmatrix} \{I(t)\} \\ q(t) \end{Bmatrix} = \begin{Bmatrix} \{P(t)\} \\ Q(t) \end{Bmatrix}, \tag{1}$$

where $\ddot{u}(t)$, $\ddot{\phi}$, $I(t)$, $q(t)$, $P(t)$ and $Q(t)$ represent the generalised accelerations, electric potential second time derivative, internal mechanical load, internal electric charge, external mechanical load and external electric charge, respectively, as functions of time t. In Eq. (1), the electric potential ϕ represents a scalar nodal field. Using displacement interpolation functions $[N]$, evaluated for each position X, the finite element mass matrix is computed from Eq. (2), as,

$$[M] = \int_V \rho [N]^T [N] dV. \tag{2}$$

where ρ represents the density of the material in the volume dV.

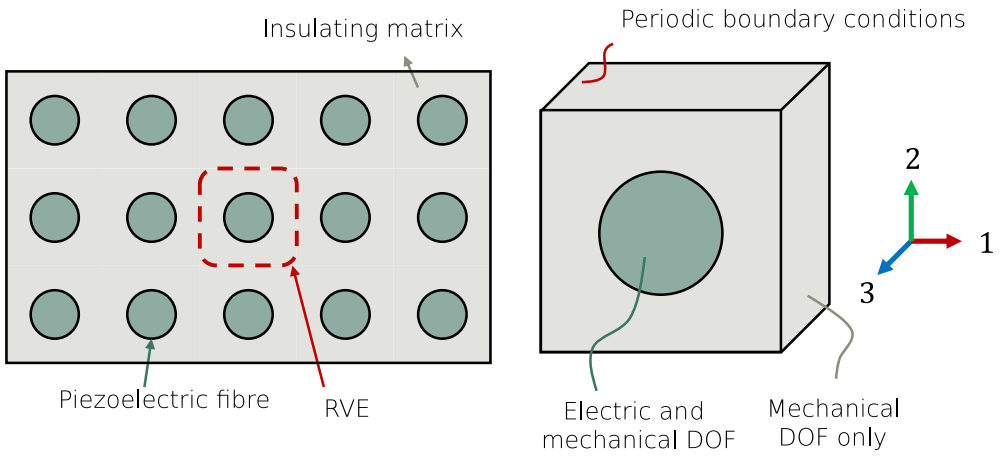

Fig. 1. Square/circular RVE.

2.1. Viscoelasticity modelling

Under linear viscoelasticity, stresses can be evaluated by the assumption of infinitesimal increases in the strain rate $\dot{\varepsilon}_{kl}$ integrated over a constitutive tensor of relaxation R_{ijkl}, as in Eq. (3). In the equation, time t represents the current instant while τ is the instant of each infinitesimal strain increment,

$$\sigma_{ij}(t) = \int_0^t R_{ijkl}(t-\tau)\frac{d\varepsilon_{kl}\ (t)}{d\tau}d\tau. \tag{3}$$

For linear viscoelastic, isotropic materials, the relaxation constitutive tensor R_{ijkl} is often described in terms of shear and bulk moduli, so that,

$$\boldsymbol{\sigma}(t) = \int_0^t 2G(t-\tau)\frac{d\boldsymbol{e}\ (t)}{d\tau}d\tau + \mathbf{I}\int_0^t K(t-\tau)\frac{d\boldsymbol{\Delta}\ (t)}{d\tau}d\tau, \tag{4}$$

where G and K are the shear and bulk relaxation moduli, while $\boldsymbol{e}$ and $\boldsymbol{\Delta}$ are the deviatoric and volumetric strains, respectively and $\mathbf{I}$ represents the second-order identity tensor. As the relaxation modulus R_{ijkl} is a function of time, the corresponding constitutive behaviour can be analysed using an exponential function applied over the time-independent elasticity tensor R^0_{ijkl}. A Prony series expansion is shown in Eq. (5) for the shear elastic modulus $G(t)$ and is usually employed for mechanical viscoelastic constitutive behaviour, where g_k are the relaxation coefficients corresponding to time τ_k. Similarly, Eq. (6) shows a Prony series expansion for the Bulk modulus $K(t)$,

$$G(t) = G_0\left[1 - \sum_{k=1}^{n} g_k\left(1 - e^{-\frac{t}{\tau_k}}\right)\right], \tag{5}$$

$$K(t) = K_0\left[1 - \sum_{k=1}^{n} k_k\left(1 - e^{-\frac{t}{\tau_k}}\right)\right]. \tag{6}$$

Therefore, the internal load vector at any given instant t for a viscoelastic material is computed from both the initial response at the initial time $u(0)$ as well as the time-dependent displacement history $u(t)$, as displayed in Eq. (7) and implemented in Wang et al. [31]. In the equation, $[B]$ represents the spatial derivative of the interpolation functions N while $R(t)$ is the time-dependent relaxation modulus.

$$\{I(t)\} = \left[\int_V [B]^T[R(t)][B]dV\right]\left\{u(0)\right\} + \int_0^t\int_V [B]^T[R(t-\tau)][B]dV\frac{d}{d\tau}\left\{u(t)\right\}d\tau. \tag{7}$$

Equivalent external nodal loads are calculated using Eq. (8) from body loads P_v and traction P_S, distributed over volume V and surfaces S, in addition to concentrated loads P_c,

$$\{P(t)\} = \int_V [N]^T\{P_v\}dV + \int_S [N]^T\{P_S\}dV + P_c. \tag{8}$$

For the proposed FE model, the viscoelastic constituent displays only mechanical degrees of freedom, so that, for the piezoelectric fibres:

$$\{q(t)\} = \{0\}. \tag{9}$$

Therefore, Eqs. (7), (8) and (9) represent the finite element vector contributions for the viscoelastic matrix on the discrete equilibrium, which will be shown by Eq. (17).

2.2. Piezoelectric modelling

Piezoelectric materials usually display linear elastic mechanical behaviour associated with an electric coupling. Therefore, the piezoelectric modelling used in this work assumes linear piezo-electricity, as represented by Eq. (10) where stress tensor σ_{ij} is a function of both the strains ε_{kl} as well as the electric field E_k, with indices i, j, k and l varying from 1 to 3. Similarly, the charge density D_i in Eq. (11) is a function of strains as well as the electric field. In Eqs. (10) and (11), C_{ijkl} is a fourth-order elasticity tensor, e_{ikl} is a third-order piezoelectricity tensor representing the electric/mechanical coupling, and η_{ij} is a second-order dielectric tensor,

$$\sigma_{ij} = C_{ijkl}\varepsilon_{kl} - e_{kij}E_k, \tag{10}$$

$$D_i = e_{ikl}\varepsilon_{kl} + \eta_{ij}E_j. \tag{11}$$

However, the microscopic arrangement of piezoelectric crystals shows some influence on the effective constitutive behaviour. In this analysis, an orthotropic piezoelectric material is assumed for the piezoelectric fibre, as discussed in Berger et al. [9], Rodríguez-Ramos et al. [12], Otero et al. [11] and Otero et al. [16]. For the FE framework, with displacement and electric potential interpolation functions, the generalised internal load vector yields

$$\begin{Bmatrix}\{I(t)\}\\ q(t)\end{Bmatrix} = \begin{bmatrix}k_{uu} & k_{u\phi}\\ k_{u\phi} & k_{\phi\phi}\end{bmatrix}\begin{Bmatrix}\{u(t)\}\\ \phi(t)\end{Bmatrix}, \tag{12}$$

where:

$$[k_{uu}] = \int_V [B]^T[C][B]dV, \tag{13}$$

$$[k_{u\phi}] = \int_V [B]^T[e][B]dV, \tag{14}$$

and

$$[k_{\phi\phi}] = \int_V [B]^T[\eta][B]dV. \tag{15}$$

External loads are also obtained from the consistent generalised nodal load vector from Eq. (16), with Q_v, Q_S and Q_c representing body,

surface and concentrated external charges,

$$\begin{Bmatrix} \{P(t)\} \\ Q(t) \end{Bmatrix} = \begin{Bmatrix} \int_V [N]^T \{P_v\} dV + \int_S [N]^T \{P_S\} dV + \{P_c\} \\ \int_V [N]^T Q_v dV + \int_S [N]^T Q_S dV + Q_c \end{Bmatrix}. \quad (16)$$

Therefore, Eqs. (12) and (16) represent the FE load vector contributions for the piezoelectric fibre, on the discrete equilibrium, which will be shown by Eq. (17). Different from the matrix, the piezoelectric fibres show contributions on both mechanical and electric degrees of freedom.

2.3. Equilibrium equations

Finite element solutions over time can be achieved through an incremental approach over the simulation time span. Therefore, an implicit time-integration scheme is employed as

$$\lambda[\mathbf{M}]\{\ddot{\mathbf{u}}_{\mathbf{t+\Delta t}}\} + (1+\alpha)\left(\{\mathbf{I}_{\mathbf{t+\Delta t}}\} + \{\mathbf{P}_{\mathbf{t+\Delta t}}\}\right) - \alpha\left(\{\mathbf{I}_{\mathbf{t}}\} + \{\mathbf{P}_{\mathbf{t}}\}\right) = 0, \quad (17)$$

where α is a dynamic relaxation parameter to improve convergence within a time increment and λ is an inertial load reduction parameter, that can either eliminate or attenuate the inertial effects, as $0 \leq \lambda \leq 1$. In Eq. (17), $\{\ddot{\mathbf{u}}_{\mathbf{t}}\}$, $\{\boldsymbol{I}_{\boldsymbol{t}}\}$ and $\{\mathbf{P}_{\mathbf{t}}\}$ represent the generalised acceleration, internal and external load vectors, evaluated at time t, while $\lambda[\mathbf{M}]$ is the generalised mass Matrix. In Eq. (17), the inertial, internal, and external loads are displayed as the generalised load vectors accounting for electric and mechanical time-dependent nodal loads. To represent the time-dependent effects of viscoelasticity only, FE models were implemented using Abaqus/*Standard*, without inertial effects ($\lambda = 0$). Under these conditions, the solution scheme implemented is a backward Euler method applied to the implicit discrete equilibrium equations.

2.4. Finite element homogenisation

The coupling of piezoelectric and viscoelastic materials results in time-dependent piezoelectric and dielectric components. Therefore, a virtual stress relaxation test is introduced, where a uniaxial strain field history is prescribed for each analysis, as represented by the Heaviside function $H(t)$

$$\varepsilon_{ij}\ (t) = \varepsilon^0_{ij}\ H(t), \quad (18)$$

where ε^0_{ij} represents the prescribed strain tensor component and stresses σ_{ij} can be computed as

$$\sigma_{ij}(t) = C_{ijkl}(t)\varepsilon_{ij}(t). \quad (19)$$

Each load case was applied using prescribed displacements and electric potential fields using a time-dependent amplitude that represents the Heaviside function. However, it is essential to note that the Heaviside function is only applicable when a static solution is required, as it leads to unbound accelerations for the initial increment. Therefore, in the presence of inertial effects ($\lambda \neq 0$), the step function might result in additional oscillations in stress magnitudes.

Considering finite element analysis, stress and strain values are computed for each m_{th} element at the corresponding n_{th} integration point ranging from 1 to n_e for the number of elements, and 1 to n_{ip} for the number of integration points. Therefore, the average stresses ($\overline{\sigma}_{ij}$), strains ($\overline{\varepsilon}_{ij}$), electric potentials ($\overline{E}_i$) and electric charge densities ($\overline{D}_i$), are computed for each integration point and averaged over the representative volume element (V) as

$$\overline{\sigma}_{ij} = \frac{1}{V}\sum_m^{n_e}\sum_n^{n_{ip}} \sigma_{ij}^{m,n}\Delta V, \quad (20)$$

$$\overline{\varepsilon}_{ij} = \frac{1}{V}\sum_m^{n_e}\sum_n^{n_{ip}} \varepsilon_{ij}^{m,n}\Delta V, \quad (21)$$

$$\overline{E}_i = \frac{1}{V}\sum_m^{n_e}\sum_n^{n_{ip}} E_i^{m,n}\Delta V \quad (22)$$

and

$$\overline{D}_i = \frac{1}{V}\sum_m^{n_e}\sum_n^{n_{ip}} D_i^{m,n}\Delta V. \quad (23)$$

Therefore, under stress relaxation, the effective instantaneous constitutive relation of the homogenised RVE is also time-dependent. Assuming a circular piezoelectric fibre embedded in a cube matrix region, the symmetry of the RVE results in the following effective time-dependent relation (see the Eq. (24) in Box I) where an orthotropic combined with a transversely isotropic effective behaviour is assumed. In Eq. (24) fifteen effective constitutive parameters are required for the characterisation of the homogenised medium.

2.5. Halpin–Tsai formulation

As the proposed methodology neglects electric potential and charge DOFs for the matrix constituent, external faces of the RVE do not allow for electric boundary conditions to be prescribed. Therefore, the 7th and 8th lines in Eq. (24) would be eliminated for the effective piezo-viscoelastic homogenised material. However, constant e_{15} represents a piezoelectric coupling between electric flux $\overline{D}_1$ and shear strains $\overline{\gamma}_{13}$ as well as $\overline{D}_2$ and $\overline{\gamma}_{23}$. Therefore, for the load cases with these scenarios (non-zero $\overline{\gamma}_{13}$ and $\overline{\gamma}_{23}$), the electric potential gradients $\overline{E}_1$ and $\overline{E}_2$ are assumed arbitrary so that

$$\overline{D}_1(t) = e_{15}^{eff}(t)\overline{\gamma}_{13} + \eta_{11}^{eff}(t)\overline{E}_1(t), \quad (25)$$

and

$$\overline{D}_2(t) = e_{15}^{eff}(t)\overline{\gamma}_{23} + \eta_{11}^{eff}(t)\overline{E}_2(t). \quad (26)$$

Therefore, piezoelectric coefficient can be extracted from either Eq. (25) or (26), given that the effective dielectric constant $\eta_{11}^{eff}(t)$ is known. To overcome the limitation in the proposed methodology, the dielectric constant is assumed as constant over time and calculated using the Halpin–Tsai analytical formulation for square/circular fibre packing,

$$\varphi = 2\left(\frac{l}{d}\right). \quad (27)$$

$$\chi = \frac{\frac{\eta_{11}^f}{\eta_{11}^m} - 1}{\frac{\eta_{11}^f}{\eta_{11}^m} + \varphi}, \quad (28)$$

as a function of the dielectric constants η_{11}^m and η_{11}^f for the fibre and the matrix, respectively. For the computation of the effective permittivity, the microstructure form factor φ is computed from the length l to diameter ratio d in Eq. (27), yielding a value of $\varphi = 2$ for the square/circular geometry. The ratio between dielectric properties is evaluated from Eq. (28) so that the effective parameter for a given fibre volume ratio V_f is

$$\eta_{11}^{eff} = \frac{1 + \chi\varphi V_f}{1 - \chi V_f}. \quad (29)$$

Finally, with the known effective dielectric constant, the effective piezoelectric coupling coefficient $e_{15}^{eff}(t)$ is calculated from Eq. (25) and elastic shear modulus $C_{44}^{eff}(t)$ is obtained from Eq. (30).

$$\overline{\sigma}_{23}(t) = C_{44}^{eff}(t)\gamma_{23} - e_{15}(t)\overline{E}_2(t). \quad (30)$$

2.6. Geometry and finite element model

The FE implementation was conducted using Abaqus/*Standard* FE code, using the dynamic equilibrium with implicit time integration solver (Dynamic/ Implicit). Second-order three-dimensional continuum elements (C3D20) were used for the viscoelastic matrix, while second-order three-dimensional piezoelectric elements (C3D20E) were used for

$$\begin{Bmatrix} \overline{\sigma}_{11}(t) \\ \overline{\sigma}_{22}(t) \\ \overline{\sigma}_{33}(t) \\ \overline{\sigma}_{12}(t) \\ \overline{\sigma}_{23}(t) \\ \overline{\sigma}_{13}(t) \\ \overline{D}_1(t) \\ \overline{D}_2(t) \\ \overline{D}_3(t) \end{Bmatrix} = \begin{bmatrix} C_{11}^{eff}(t) & C_{12}^{eff}(t) & C_{13}^{eff}(t) & 0 & 0 & 0 & 0 & 0 & -e_{13}^{eff} \\ C_{12}^{eff}(t) & C_{11}^{eff}(t) & C_{13}^{eff}(t) & 0 & 0 & 0 & 0 & 0 & -e_{13}^{eff} \\ C_{13}^{eff}(t) & C_{13}^{eff}(t) & C_{33}^{eff}(t) & 0 & 0 & 0 & 0 & 0 & -e_{33}^{eff}(t) \\ 0 & 0 & 0 & C_{66}^{eff}(t) & 0 & 0 & 0 & 0 & 0 \\ 0 & 0 & 0 & 0 & C_{44}^{eff}(t) & 0 & 0 & -e_{15}^{eff}(t) & 0 \\ 0 & 0 & 0 & 0 & 0 & C_{44}^{eff}(t) & -e_{15}^{eff}(t) & 0 & 0 \\ 0 & 0 & 0 & 0 & 0 & e_{15}^{eff}(t) & \eta_{11}^{eff}(t) & 0 & 0 \\ 0 & 0 & 0 & 0 & e_{15}^{eff}(t) & 0 & 0 & \eta_{11}^{eff}(t) & 0 \\ e_{13}^{eff}(t) & e_{13}^{eff}(t) & e_{33}^{eff}(t) & 0 & 0 & 0 & 0 & 0 & \eta_{33}^{eff}(t) \end{bmatrix} \begin{Bmatrix} \overline{\varepsilon}_{11} \\ \overline{\varepsilon}_{22} \\ \overline{\varepsilon}_{33} \\ \overline{\gamma}_{12} \\ \overline{\gamma}_{23} \\ \overline{\gamma}_{13} \\ \overline{E}_1 \\ \overline{E}_2 \\ \overline{E}_3 \end{Bmatrix}, \tag{24}$$

Box I.

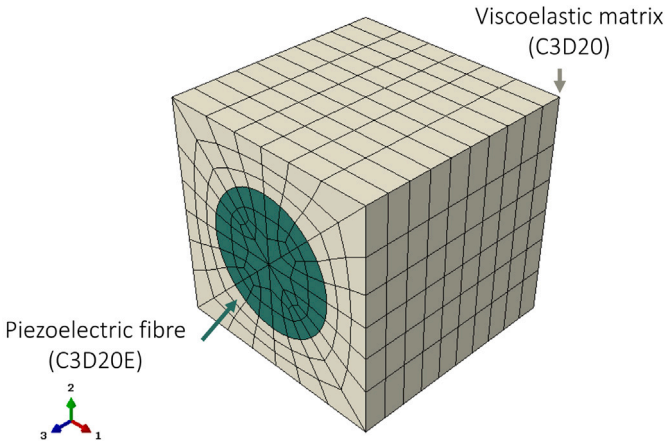

Fig. 2. Square/circular RVE.

the piezoelectric fibre. Compatibility between fibre and matrix was naturally enforced through the generation of a single mesh using geometry partitions, therefore not requiring complex interaction constraints at the interfaces (see Fig. 2).

To better represent the constraints acting on the RVE, Periodic Boundary Conditions (PBCs) were enforced over external surfaces. A node-by-node PBC algorithm was employed using the methodology proposed by [29] and further explored by [25]. Displacement of nodes on opposite faces of the RVE is related to each other, thus satisfying the boundary conditions. Assuming displacement component i between opposite faces $k+$ and $k-$, displacements are

$$u_i^{k+} - u_i^{k-} = \overline{\varepsilon}_{ij}\left(x_j^{k+} - x_j^{k-}\right), \tag{31}$$

where $\overline{\varepsilon}_{ij}$ is the prescribed strain while x_j^{k+} and x_j^{k-} are the j_{th} component of the position vector of each nodes. Within the FE framework, PBCs are enforced only over the displacement field as traction continuity is naturally satisfied. However, for a piezoelectric element, electric potentials ϕ are represented as part of the generalised displacement vector. Therefore, the distinction between displacements and potentials is made here, so that PBCs for the electric degrees of freedom become

$$\phi_i^{k+} - \phi_i^{k-} = \overline{E}_i(x_j^{k+} - x_j^{k-}). \tag{32}$$

In addition to the PBCs, displacements were prescribed in the model, producing uniaxial strain fields required for the numerical homogenisation procedure employed. The prescribed displacement and corresponding strains were enforced as a step function and maintained constant during the analysis. For the simulated scenarios, a total time $t = 200$ s was chosen. Similar to the methodology presented in Berger et al. [9], multiple load cases were prescribed and effective constitutive coefficients computed throughout time. In total, five load cases were implemented to produce the following uniaxial fields: $\overline{\varepsilon}_{11}$, $\overline{\varepsilon}_{33}$, $\overline{\gamma}_{23}$, $\overline{\gamma}_{12}$, and $\overline{E}_3$.

2.7. Asymptotic homogenisation method considering viscoelastic effects

The asymptotic homogenisation method is a powerful analytical-numerical technique used to determine the effective properties of heterogeneous materials with periodic or quasi-periodic microstructures [32]. This method enables the derivation of averaged, or homogenised, physical properties such as elastic moduli, thermal conductivities, or diffusivities from the detailed behaviour of the material at the micro-scale. By leveraging multi-scale expansion based on a small parameter that characterises the scale separation between the microstructure and the material behaviour, the method provides an accurate approximation of the effective behaviour of media with rapidly oscillating material coefficients. The homogenised properties are obtained from the knowledge of the local constitutive laws, the intrinsic properties of the constituent phases, their volume fractions, and the geometric configuration of the microstructural inclusions or reinforcements [33,34]. This approach is especially useful in engineering and materials science, where it offers significant computational advantages over direct numerical simulations of the full heterogeneous domain, while still capturing essential features of the microstructure in the macroscopic response.

The expressions for the effective coefficients previously reported in Guinovart-Díaz et al. [35], Guinovart-Díaz et al. [36], and Bravo-Castillero et al. [37], derived using the asymptotic homogenisation method, were extended to the case presented previously, where a piezoelectric fibre is embedded in a viscoelastic matrix. These effective properties are calculated for a two-phase composite material consisting of cylindrical fibres aligned along the x_3-axis and embedded within a continuous matrix. The spatial arrangement of the fibres allows the consideration of both square and hexagonal periodic unit cells, reflecting typical microstructural configurations found in engineering composites. In this extended framework, the matrix is assumed to be an isotropic viscoelastic material, while reinforcements may exhibit piezoelectric behaviour. The asymptotic homogenisation technique enables the systematic substitution of the local material properties into the cell problems, leading to closed-form expressions or numerically explicit formulas for the effective (homogenised) coefficients. Specifically, appropriate constitutive relationships and time-dependent material parameters are incorporated into the homogenisation scheme, and the corresponding viscoelastic and piezoelectric contributions are accounted for. To implement this extension, material tensors and field variables corresponding to the piezoviscoelastic behaviour are introduced into the

Table 1
Constituents' mechanical, piezoelectric and dielectric properties for static analysis [9].

	Fibre	Matrix
C_{11} (GPa)	121	3.86
C_{12} (GPa)	75.4	2.57
C_{13} (GPa)	75.2	2.57
C_{33} (GPa)	111.1	3.86
C_{44} (GPa)	21.1	0.64
C_{66} (GPa)	22.8	0.64
e_{15} (C/m^2)	12.3	–
e_{13} (C/m^2)	−5.4	–
e_{33} (C/m^2)	15.8	–
η_{11} (nF/m)	8.11	0.007965
η_{33} (nF/m)	7.35	0.007965

existing formulations. These modified expressions are then substituted into the homogenisation framework developed in the [35–37], thereby enabling the evaluation of the macroscopic response of the composite material under coupled mechanical and electrical loading conditions. It is assumed that the matrix is an isotropic viscoelastic material, and the following expressions are substituted into the corresponding formulas reported in the above references,

$$\begin{aligned} C_{11}^{\mathrm{m}} = C_{33}^{\mathrm{m}} &= K_0 + \frac{4}{3}\mu_0(p), \\ C_{12}^{\mathrm{m}} = C_{13}^{\mathrm{m}} &= K_0 - \frac{2}{3}\mu_0(p), \\ C_{44}^{\mathrm{m}} = C_{66}^{\mathrm{m}} &= \mu_0(p), \end{aligned} \tag{33}$$

where K_0 and μ_0 represent the instantaneous bulk and shear moduli of the matrix material, evaluated at the initial instant. Also, it is possible to define:

$$\mu_0(p) = \mu_0\left(1 + \frac{\lambda}{\beta + p^{1-\alpha}}\right). \tag{34}$$

If the matrix is isotropic, it is possible denotes the bulk K_0 and shear μ_0 elastic moduli. Moreover,

$$\beta = \frac{1}{\tau^{1-\alpha}}, \quad \lambda = \beta\left(1 - \varepsilon_{\max}\right) = \frac{\mu_\infty - \mu_0}{\mu_0}\beta, \tag{35}$$

where $0 \leq \alpha \leq 1$, τ is relaxation time, μ_∞ is the shear modulus at $\tau \to \infty$, μ_0 is instantaneous shear modulus, and $\varepsilon_{\max}$ is maximal shear strain. Thus, viscoelastic shear behaviour of a material is described by four parameters: μ_0, α, β (or τ), and λ. Further details are provided in Otero et al. [16].

Finally, the inverse Laplace-Carson transform is applied to the expressions of the effective coefficients in the Laplace-Carson space denoted by the variable p, and the time behaviour of the effective coefficients is obtained [11,12].

2.8. Application of the methodology

The application of the proposed methodology was carried out in two scenarios. First, the static response of linear piezoelectric composite materials with different fibre volume ratios was compared to the analytical and finite element results extracted from Berger et al. [9], using a square/circular fibre packing configuration. However, the methodology proposed here, disregards electric degrees of freedom for the matrix, uses a node-to-node PBC scheme, and computes effective constitutive properties at the first increment of the dynamic equilibrium solution. The constituent properties used in this validation are displayed in Table 1.

Following the validation of the proposed procedure on a static load case, viscoelastic effective properties were computed using the finite element homogenisation procedure, over time, and compared to effective field results. Table 2 displays the elastic, piezoelectric and dielectric properties of the materials for each constituent.

Table 2
Constituents' elastic, piezoelectric and dielectric properties for time-dependent analysis.

	Fibre	Matrix
C_{11} (GPa)	150.4	7.73
C_{12} (GPa)	65.63	5.15
C_{13} (GPa)	65.94	5.15
C_{33} (GPa)	145.5	7.73
C_{44} (GPa)	43.86	1.29
C_{66} (GPa)	42.385	1.29
e_{15} (C/m^2)	11.4	–
e_{13} (C/m^2)	−4.32	–
e_{33} (C/m^2)	17.4	–
η_{11} (nF/m)	12.8	0.0443
η_{33} (nF/m)	12.8	0.0443

Table 3
Prony series coefficients for viscoelastic matrix.

t [s]	9.6	372	9887
g_k [–]	0.03807	0.0458	0.0668
k_k [–]	0	0	0

In addition, Prony series coefficients for the viscoelastic matrix are displayed in Table 3, so that only the deviatoric part of the strain tensor contributes to the viscoelastic behaviour. This is representative of an epoxy matrix, commonly used in Macro Fibre Composite (MFC) and smart sensors [3].

3. Results and discussion

In this section, results obtained through the proposed FE-based homogenisation are compared to analytical solutions using effective field and asymptotic homogenisation methods (AHM) for piezoviscoelastic composite materials. In this work, the validations are performed using the AHM reported in Otero et al. [11], for the elastic case ($t = 0$), and a comparison is also made with the effective field presented in Otero et al. [16].

3.1. Linear elastic results

For a uniaxial strain field $\overline{\varepsilon}_{33}$, obtained through displacements prescribed along the fibre direction, different stress values are expected for each constituent. Fig. 3(a) shows the predicted stress field under this condition, at a given instant for a fibre volume ratio $V_f = 0.4$, assuming zero electric potential at all faces of the RVE.

As expected, due to the constitutive stiffness mismatch between the constituents, the fibre exhibits greater stresses compared to the matrix. Additionally, due to the constraint on electric potential, electric flux $\overline{D}_3$ develops, as shown in Fig. 3(b). From the image, it becomes clear that the proposed approach assumes an insulating matrix without electric degrees of freedom.

Similarly, under a non-zero shear strain field γ_{23}, different stress magnitudes are predicted for each material, as displayed in Fig. 4(a). However, a strong piezoelectric coupling is expected under such conditions. As the proposed methodology does not allow for electric potential gradients to be prescribed for either $\overline{E}_1$ and $\overline{E}_2$, such fields were assumed as arbitrary and taken into account for the post-processing of effective constitutive properties. Fig. 4(b) displays the non-zero electric potential gradient field $\overline{E}_2$ for the shear load case, at the same instant from Fig. 4(a).

Correlation between the effective constitutive coefficients obtained by the proposed model and analytical results is displayed in Fig. 5, for elastic and piezoelectric parameters C_{11}, C_{12}, C_{13}, C_{33}, C_{44}, C_{66}, e_{15}, e_{13}, and e_{33}. The predictions are also compared to Finite Element Method (FEM) results reported in [9], considering linear elastic piezoelectric elements in a linear static analysis, disregarding viscoelastic effects.

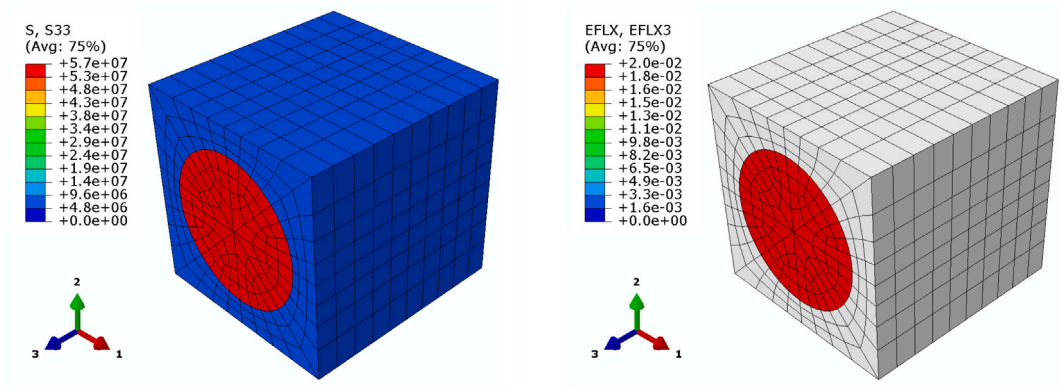

(a) Normal stress σ_{33} in N/m^2. (b) Electric flux D_3 in C/m^2.

Fig. 3. Stress and electric flux fields for non-zero ϵ_{33} - $V_f = 0.4$.

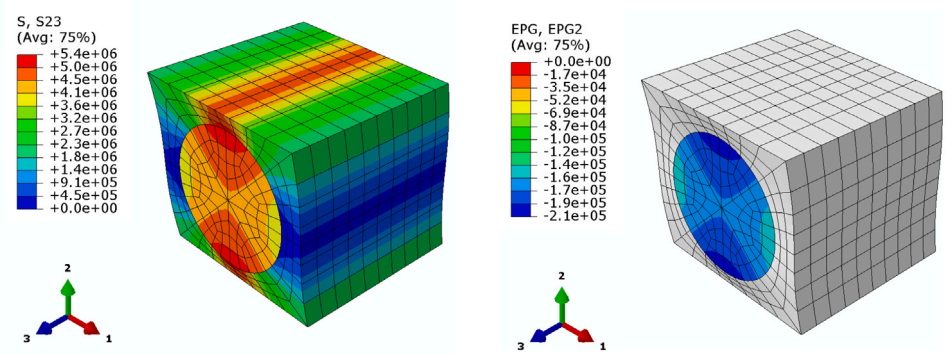

(a) Shear stress σ_{23} in N/m^2. (b) Electric potential gradient E_2 in V/m.

Fig. 4. Stress and electric potential gradient fields for non-zero γ_{23} - $V_f = 0.4$.

Different from the conventional methodology, the proposed method prescribed PBC's using a node-to-node formulation and yielded results in accordance with AHM analytical solutions. Therefore, the proposed methodology can capture static results even with a time-dependent solution methodology coupled with an insulating matrix behaviour. Moreover, even for static responses, evaluated at $t = 0$, there are differences between FE based and analytical homogenisation results, as seen for grater fibre volume ratios V_f for components C_{11}, C_{12}, C_{44}, C_{66} and e_{15}, where the viscoelastic effects can influence not only the mechanical coefficients, but also the piezoelectric coefficient related to shear strains.

3.2. Viscoelastic results

At any given instant, effective constitutive coefficients were computed for the time-dependent matrix material behaviour. As the strain and electric potential gradient fields were prescribed over time, stress and electric flux fields also showed time-dependent behaviour. Fig. 6 shows stresses σ_{11} (a) for uniaxial field $\overline{\varepsilon}_{11}$, σ_{33} (b) and D_3 (e) for $\overline{\varepsilon}_{33}$, σ_{23} (c) and E_2 (e) for $\overline{\gamma}_{23}$ and σ_{12} (d) for non-zero $\overline{\gamma}_{12}$ at the final time $t = 200$ s.

A mesh independence analysis was performed to ensure that the viscoelastic response is not affected by the finite element mesh density throughout the simulation time. Therefore, five different global element size values were evaluated, yielding discretisations with 40, 80, 224, 1360, and 2490 elements, respectively. Fig. 7 shows the effective coefficients C_{44} and e_{15} computed for the volume fraction of 20%, where the viscoelastic effect is higher. The analysis showed that for models with $N_{el} \geq 1360$, convergence was achieved for the piezoelectric coupling constant e_{15}. Therefore, all the following results are displayed for meshes with 1360 elements, as they provided accurate results at a lower computational cost.

When analysing the FE predictions at the first increment at $t = 0$, static solutions are obtained, similarly to solutions discussed in Section 3. Fig. 8 shows the comparison between analytical results obtained through effective field homogenisation and the proposed methodology as a function of fibre volume ratio V_f. Results showed a similar dependency on fibre volume ratio, with small differences for higher values of V_f only.

The effect of different fibre volume ratios on the constitutive component C_{33} is shown in Fig. 9 throughout time, where dots represent the FE results and lines represent the AHM analytical response. From the image, it is clear that approximately no time-dependent behaviour occurs under these conditions, as the deviatoric strain components are negligible, thus inhibiting stress relaxation. Similarly, Fig. 10 shows that the effective piezoelectric constant e_{33} is also not time-dependent for normal strain fields.

Piezoelectric coupling for extension along direction 3, e_{13} also showed negligible time-dependency, as displayed in Fig. 11. A small viscoelastic effect is observable for small V_f values, as the matrix is the only viscoelastic constituent for the composite RVE. This behaviour is observed as the Prony series parameters for time-dependent bulk modulus k_k are all prescribed as zero. Therefore, time-dependency is higher for components related to shear stresses and deviatoric strain components.

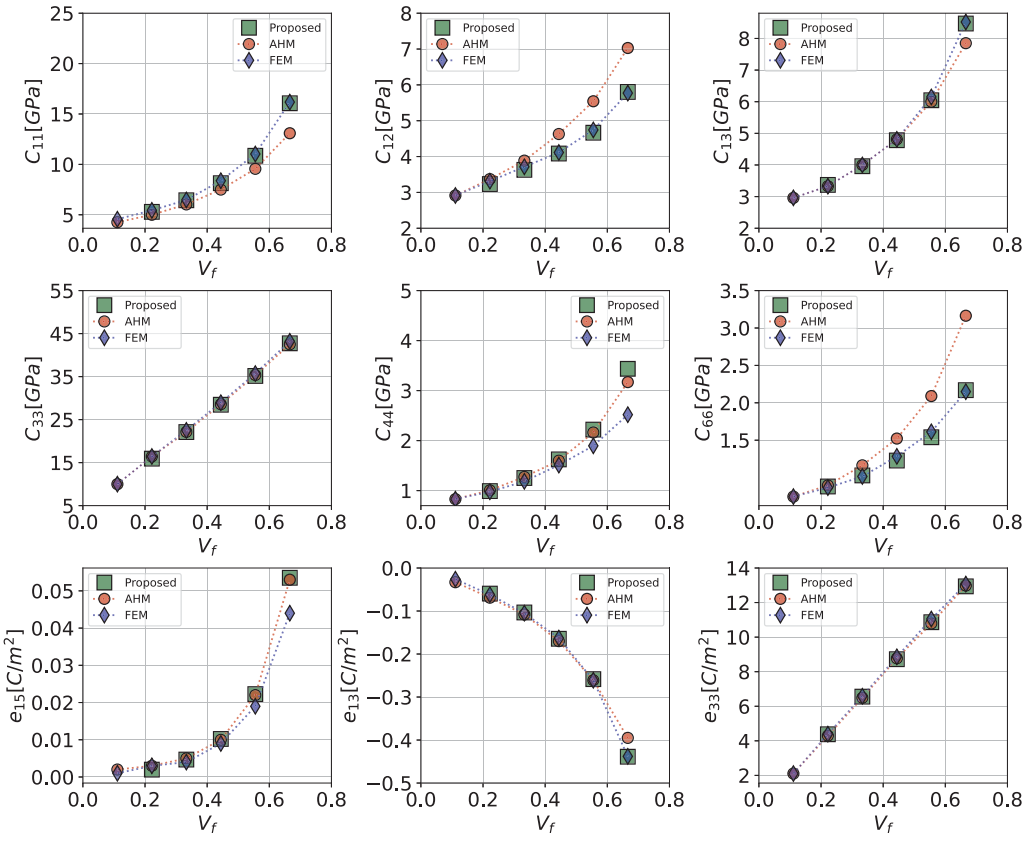

Fig. 5. Fibre volume ratio dependency at $t = 0$ s compared for static solutions: Proposed Methodology vs. AHM vs. FEM results.

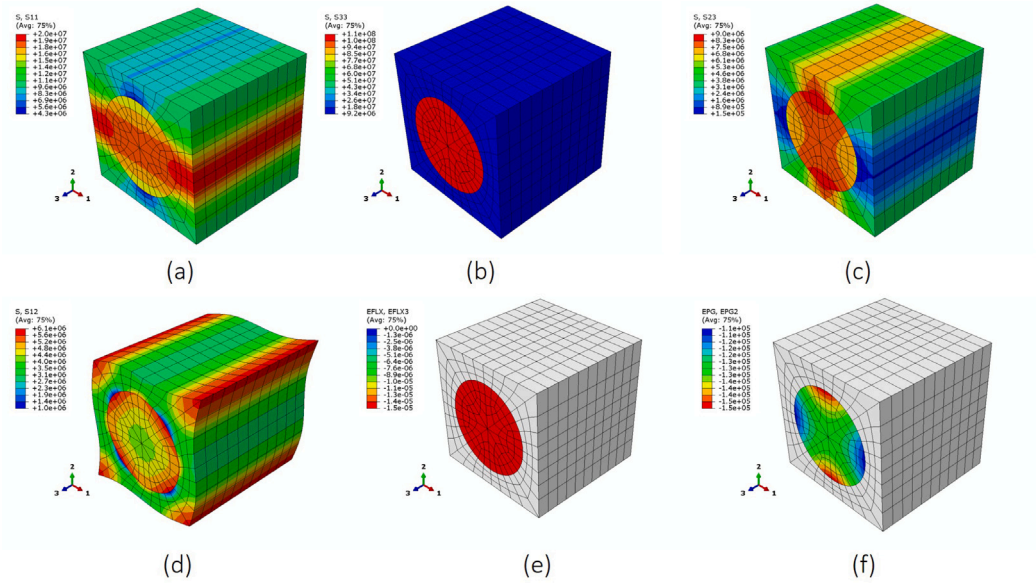

Fig. 6. Mechanical and electric fields at a given instant.

When analysing the effective constitutive properties under shear strains, time dependency is observed, as displayed in Fig. 12 for the case with non-zero $\overline{\gamma}_{12}$. As shown in the plot (Fig. 12), the proposed methodology was able to accurately represent viscoelastic behaviour when compared to the analytical methodology. This load case leads to a mechanical-only response, as piezoelectric coupling coefficient does not play a significant role.

Differently, Figs. 13 and 14 show the effective constitutive coefficients C_{44} and e_{15}, which are computed from the same self-interacting electric/mechanical load case. Shear stiffness coefficient C_{44} predicted by the proposed FE methodology showed results in agreement with AHM procedure for smaller fibre volume fractions. As V_f increases, a larger discrepancy is observed between the methods, similar to linear elastic piezoelectric results presented in Section 3.1.

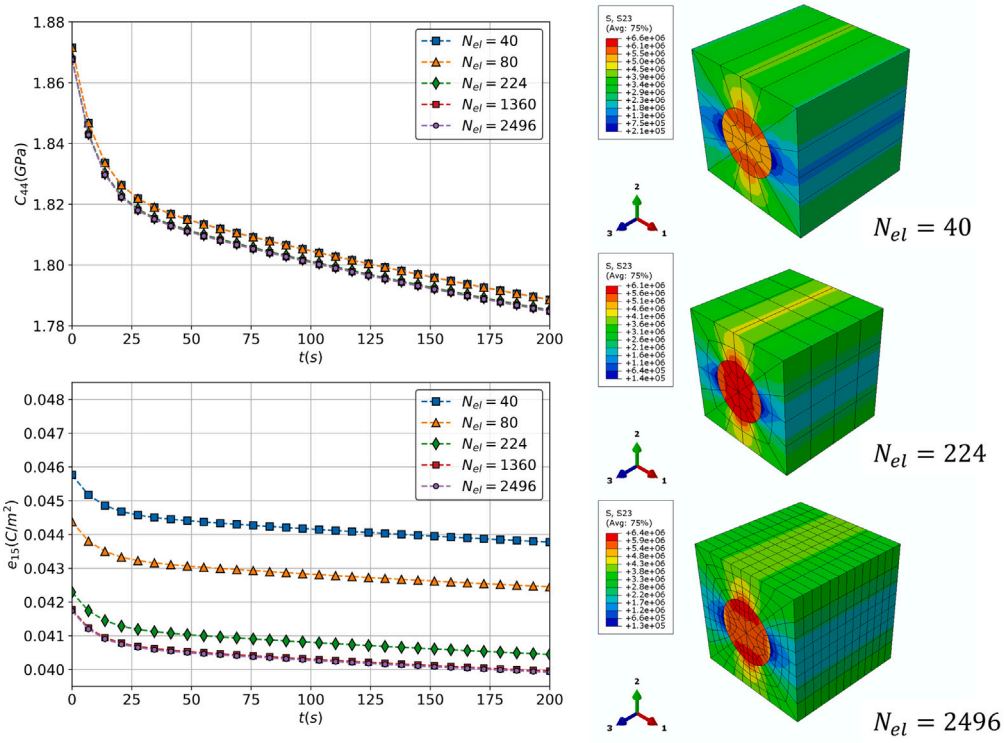

Fig. 7. Mesh dependency for effective coefficients C_{44} and e_{15}.

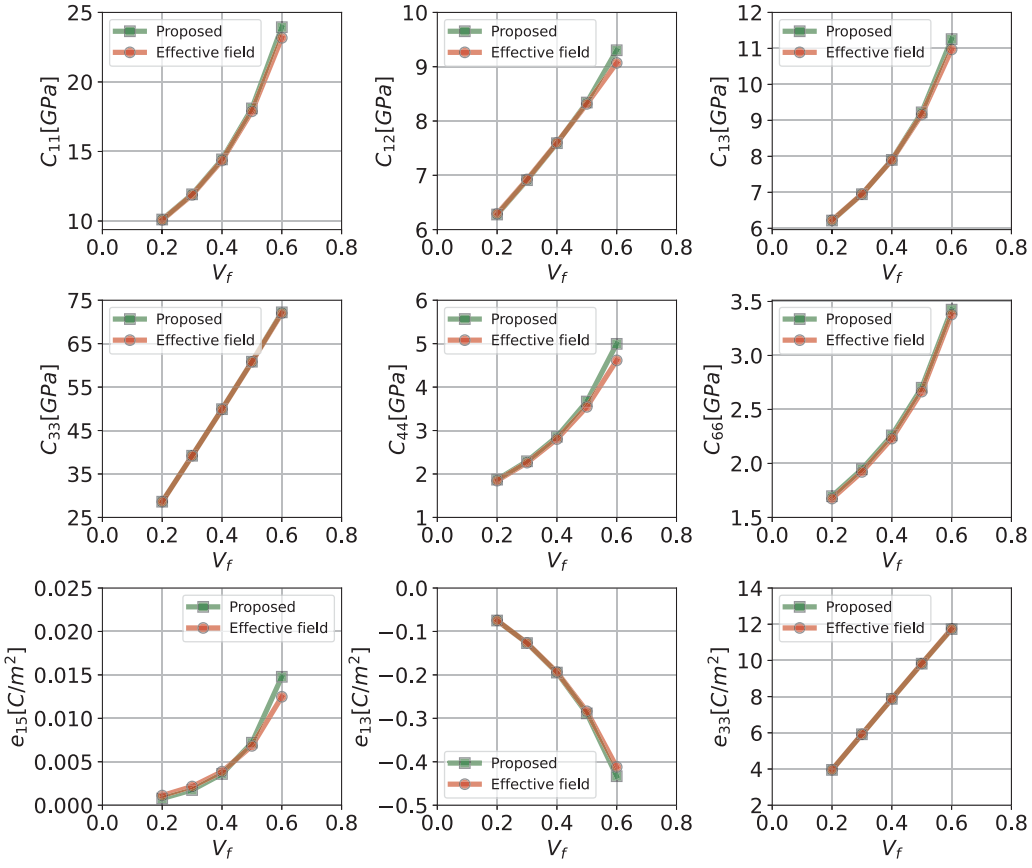

Fig. 8. Fibre volume ratio dependency at $t = 0$ s: Proposed methodology vs. AHM with viscoelastic effects.

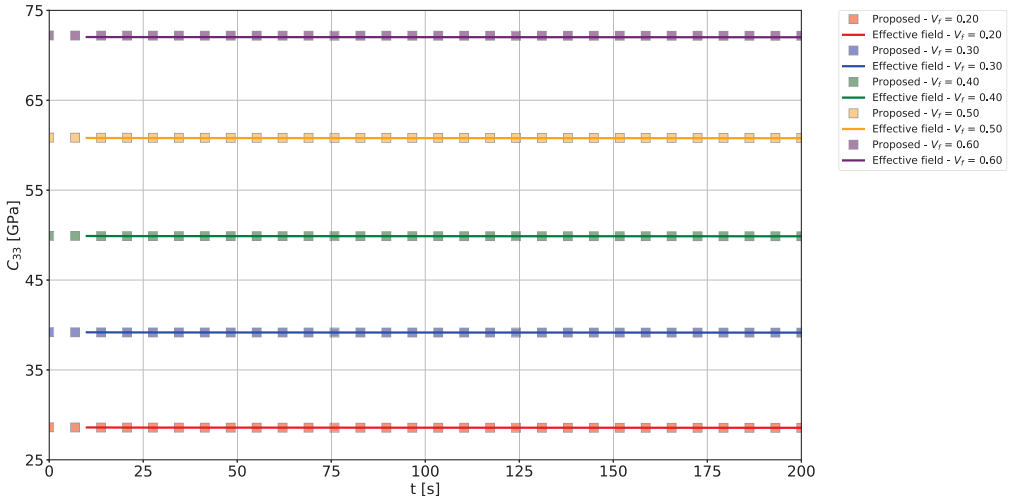

Fig. 9. Effect of different V_f on effective time-dependent constant C_{33}: Proposed methodology vs. AHM with viscoelastic effects.

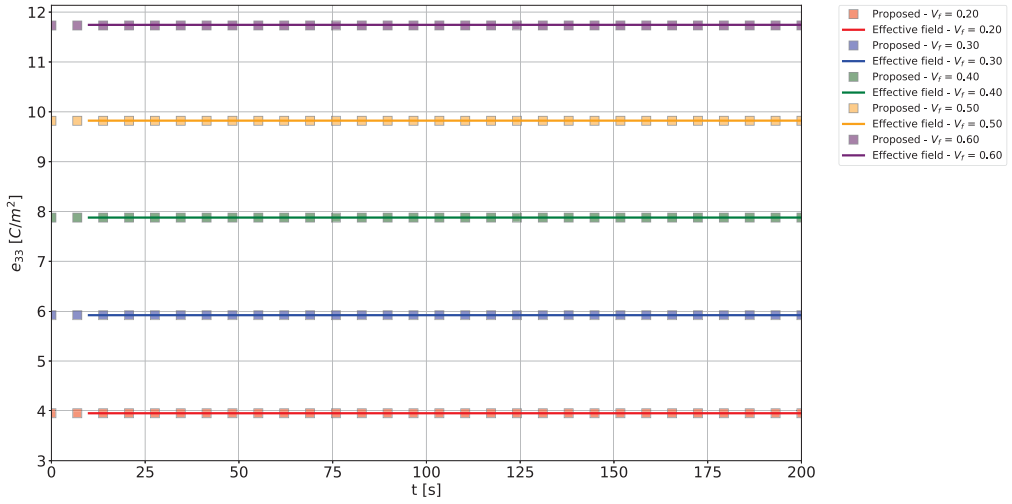

Fig. 10. Effect of different V_f on effective time-dependent constant e_{33}: Proposed methodology vs. AHM with viscoelastic effects.

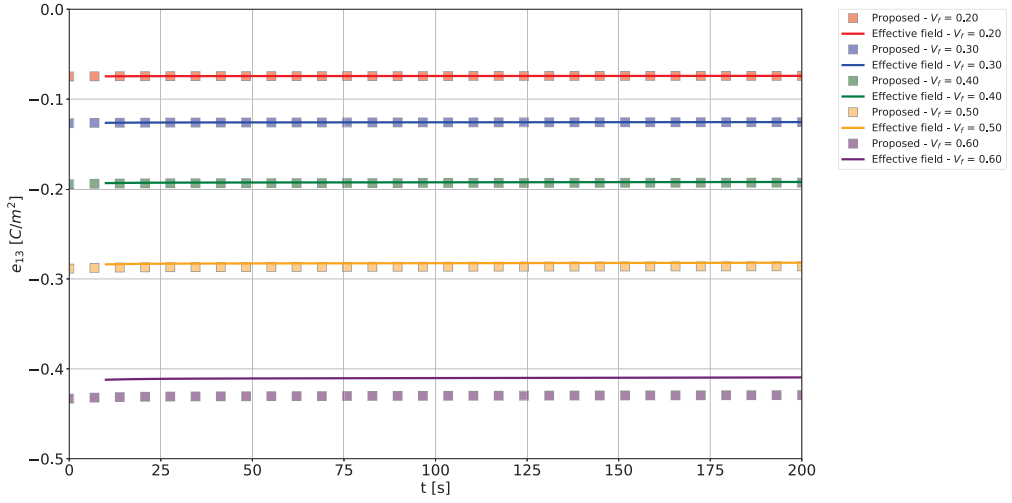

Fig. 11. Effect of different V_f on effective time-dependent constant e_{13}: Proposed methodology vs. AHM with viscoelastic effects.

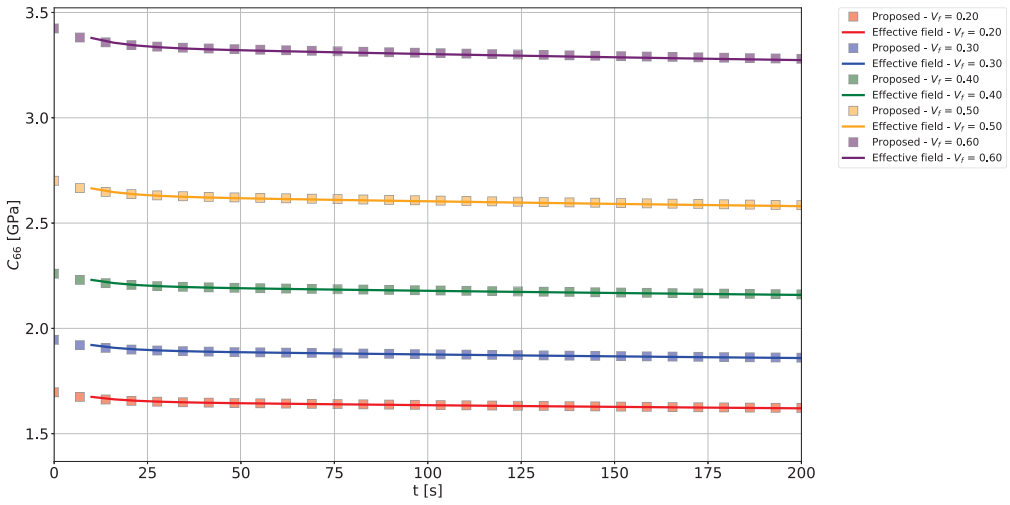

Fig. 12. Effect of different V_f on effective time-dependent constant C_{66}: Proposed methodology vs. AHM with viscoelastic effects.

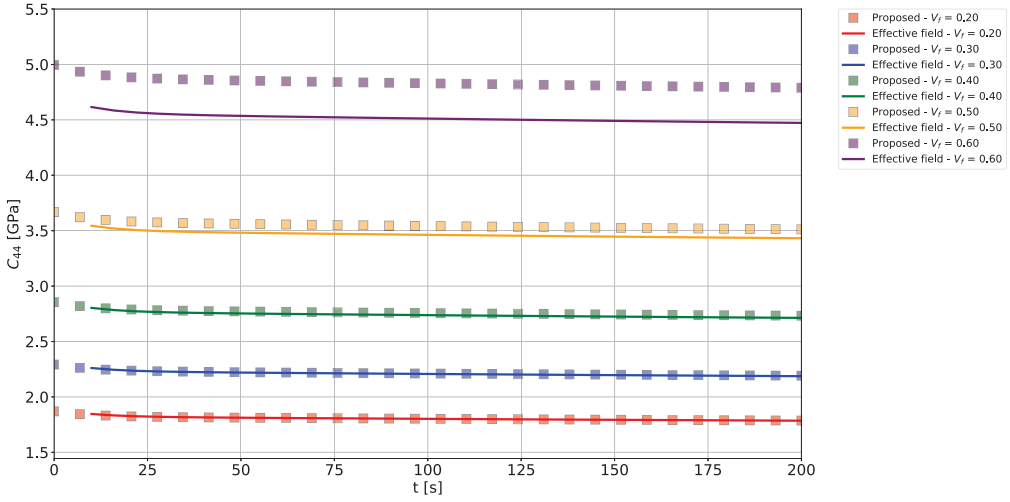

Fig. 13. Effect of different V_f on effective time-dependent constant c_{44}: Proposed methodology vs. AHM with viscoelastic effects.

Despite the assumption of an insulating matrix without electric degrees of freedom along the external faces of the RVE, post-processing of piezoelectric coupling e_{15} resulted in similar results when compared to the effective field predictions. This coefficient showed a noticeable viscoelastic response, even for higher fibre volume ratios. The proposed methodology, using the Halpin–Tsai model to compute a constant η_{11}^{eff}, resulted in a valid approximation for the piezoelectric constant with an over-prediction at lower V_f and an under-prediction at greater V_f values. This indicates that different analytical methods for estimating η_{11}^{eff} as time-dependent dielectric properties enable the improvement of the accuracy in the proposed FE homogenisation procedure.

4. Conclusions

This work successfully introduced and evaluated a novel FE-based homogenisation methodology for determining the effective constitutive and piezoelectric properties of viscoelastic composite materials. By formulating the finite element solution as a dynamic equilibrium problem, the methodology consistently captured the coupled response of linear elastic piezoelectric fibres embedded in a viscoelastic matrix, thereby accounting for the inherent time-dependent behaviour of such systems.

The proposed approach demonstrated strong agreement with analytical predictions from effective field and asymptotic homogenisation methods, even under the simplifying assumption of an insulating matrix with purely mechanical degrees of freedom. Moreover, by integrating the Halpin–Tsai model for effective dielectric behaviour, the methodology provided accurate estimations of complex piezoelectric coupling coefficients, particularly e_{15}, across a wide range of fibre volume fractions.

Beyond validating its predictive capability, this study highlights the robustness and versatility of the framework for addressing multi-scale piezo-electromechanical problems in smart materials and adaptive structures. The formulation is compatible with commercial FE codes, which broadens its applicability for engineering practice and accelerates its potential transfer to industrial contexts.

Nevertheless, some limitations remain, particularly the restriction to linear viscoelasticity and the assumption of a non-polarisable polymeric matrix. Future work should address these aspects by extending the methodology to nonlinear viscoelastic behaviour, temperature-dependent properties, and multi-fibre configurations, as well as exploring experimental validation for real composite systems.

In summary, this contribution establishes a solid foundation for FE-based micromechanical simulations of piezoviscoelastic composites and opens new avenues for the design and optimisation of advanced multifunctional materials and devices.

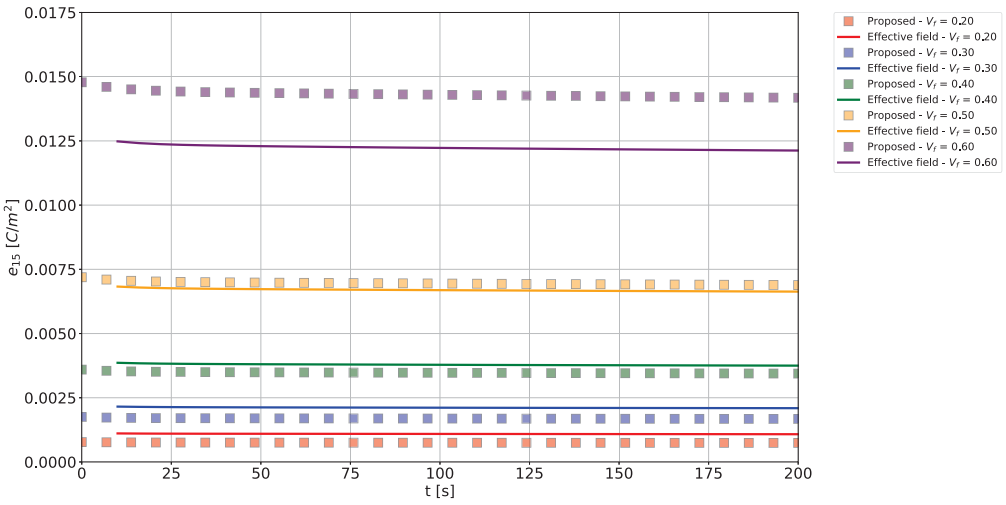

Fig. 14. Effect of different V_f on effective time-dependent constant e_{15}: Proposed methodology vs. AHM with viscoelastic effects.

CRediT authorship contribution statement

Felipe Ruivo Fuga: Writing – review & editing, Writing – original draft, Visualization, Validation, Software, Methodology, Investigation, Formal analysis, Conceptualization. **Yunior Muñoz Naranjo:** Visualization, Software, Methodology, Investigation, Formal analysis. **Reinaldo Rodríguez-Ramos:** Writing – review & editing, Supervision, Methodology, Investigation, Formal analysis, Conceptualization. **José Antonio Otero:** Writing – review & editing, Validation, Methodology, Formal analysis, Conceptualization. **Volnei Tita:** Writing – review & editing, Supervision, Project administration, Methodology, Funding acquisition, Conceptualization. **Ricardo De Medeiros:** Writing – review & editing, Writing – original draft, Validation, Supervision, Resources, Project administration, Methodology, Investigation, Funding acquisition, Formal analysis, Conceptualization.

Declaration of competing interest

The authors declare that they have no known competing financial interests or personal relationships that could have appeared to influence the work reported in this paper.

Acknowledgements

The authors acknowledge the financial support of the Santa Catarina State Research and Innovation Foundation (FAPESC numbers: 2017TR1747, 2023TR563, and 2024TR2327). As well as Coordination for the Improvement of Higher-Level Personnel (CAPES Finance Code 001). Felipe Ruivo Fuga acknowledges the financial support of the National Council for Scientific and Technological Development (CNPq), Brazil grant number: 385856/2024-5. Yunior Muñoz Naranjo acknowledges Santa Catarina Shelter Foundation from Brazil (FAPESC) grant number 734/2024. R. Rodriguez-Ramos thanks CNPq Call No. 09/2023 PQ-2 Research Productivity, process no. 307188/2023-0 and UFF PROPPI NOTICE No. 05/2022. Ricardo De Medeiros acknowledges the financial support of CNPq process number: 304795/2022-4. Volnei Tita is thankful the Brazilian Research Agencies CNPq 406148/2022-8 and 310159/2022-9, FAPEMIG and CAPES through the INCT-EIE for the financial support provided for this research effort.

Data availability

No data was used for the research described in the article.

References

[1] V. Tita, R. de Medeiros, F.D. Marques, M.E. Moreno, Effective properties evaluation for smart composite materials with imperfect fiber–matrix adhesion, J. Compos. Mater. 49 (29) (2015) 3683–3701, http://dx.doi.org/10.1177/0021998314568328.

[2] G. Wang, M. Li, J. Zhang, Z. Liang, Z. Shen, L. Liu, Z. Jiang, X. Chen, H. Song, Flexible, stable and durable polydopamine@ lead zirconate titanate/polyimide composite membranes for piezoelectric pressure sensors and limb motion monitoring, Compos. Part C: Open Access 8 (2022) 100292, http://dx.doi.org/10.1016/j.jcomc.2022.100292.

[3] M.R. Silva, V. Tita, R.D. Medeiros, Influence of the geometric parameters on the effective properties of piezoelectric composite sensors using real measurements and a new RVE, Compos. Struct. 303 (2023) 116292, http://dx.doi.org/10.1016/j.compstruct.2022.116292.

[4] Y. Wan, L. Xie, K. Lou, X. Zhang, Z. Zhong, Experimental and theoretical study on time dependence of the quasi-piezoelectric d33 coefficients of cellular piezoelectret film, J. Mech. Phys. Solids 60 (2012) 1310–1329, http://dx.doi.org/10.1016/j.jmps.2012.03.006.

[5] K. Li, X.-L. Gao, A.K. Roy, Micromechanical modeling of viscoelastic properties of carbon nanotube-reinforced polymer composites, Mech. Adv. Mater. Struct. 13 (2006) 317–328, http://dx.doi.org/10.1080/15376490600583931.

[6] A.H. Muliana, A micromechanical formulation for piezoelectric fiber composites with nonlinear and viscoelastic constituents, Acta Mater. 58 (2010) 3332–3344, http://dx.doi.org/10.1016/j.actamat.2010.02.007.

[7] H. Li, B. Zhang, A new viscoelastic model based on generalized method of cells for fiber-reinforced composites, Int. J. Plast. 65 (2015) 22–32, http://dx.doi.org/10.1016/j.ijplas.2014.08.012.

[8] H. Zhai, T. Bai, Q. Wu, N. Yoshikawa, K. Xiong, C. Chen, Time-domain asymptotic homogenization for linear-viscoelastic composites: Mathematical formulae and finite element implementation, Compos. Part C: Open Access 8 (2022) 100248, http://dx.doi.org/10.1016/j.jcomc.2022.100248.

[9] H. Berger, M. Würkner, J.A. Otero, R. Guinovart-Díaz, J. Bravo-Castillero, R. Rodríguez-Ramos, Unit cell models of viscoelastic fibrous composites for numerical computation of effective properties, in: Advanced Structured Materials, Vol. 89, Springer Verlag, 2018, pp. 69–82, http://dx.doi.org/10.1007/978-3-319-72440-9_5.

[10] O. Cruz-González, R. Rodríguez-Ramos, J. Otero, A. Ramírez-Torres, R. Penta, F. Lebon, On the effective behavior of viscoelastic composites in three dimensions, Internat. J. Engrg. Sci. 157 (2020) 103377, http://dx.doi.org/10.1016/j.ijengsci.2020.103377.

[11] J.A. Otero, R. Rodríguez-Ramos, R. Guinovart-Díaz, O.L. Cruz-González, F.J. Sabina, H. Berger, T. Böhlke, Asymptotic and numerical homogenization methods applied to fibrous viscoelastic composites using Prony's series, Acta Mech. 231 (2020) 2761–2771, http://dx.doi.org/10.1007/s00707-020-02671-1.

[12] R. Rodríguez-Ramos, J. Otero, O. Cruz-González, R. Guinovart-Díaz, J. Bravo-Castillero, F. Sabina, P. Padilla, F. Lebon, I. Sevostianov, Computation of the relaxation effective moduli for fibrous viscoelastic composites using the asymptotic homogenization method, Int. J. Solids Struct. 190 (2020) 281–290, http://dx.doi.org/10.1016/j.ijsolstr.2019.11.014.

[13] L. Azrar, A. Bakkali, A. Aljinaidi, Frequency and time viscoelectroelastic effective properties modeling of heterogeneous and multi-coated piezoelectric composite materials, Compos. Struct. 113 (2014) 281–297, http://dx.doi.org/10.1016/j.compstruct.2014.03.029.

[14] F. Vogel, S. Göktepe, P. Steinmann, E. Kuhl, Modeling and simulation of viscous electro-active polymers, Eur. J. Mech. A Solids 48 (2014) 112–128, http://dx.doi.org/10.1016/j.euromechsol.2014.02.001.

[15] J. Li, Z. Zhu, L. Fang, S. Guo, U. Erturun, Z. Zhu, J.E. West, S. Ghosh, S.H. Kang, Analytical, numerical, and experimental studies of viscoelastic effects on the performance of soft piezoelectric nanocomposites, Nanoscale 9 (2017) 14215–14228, http://dx.doi.org/10.1039/C7NR05163H.

[16] J.A. Otero, R. Rodríguez-Ramos, Y. Espinosa-Almeyda, F.J. Sabina, V. Levin, Homogenization approaches for the effective characteristics of fractional visco-piezoelastic fibrous composites, Acta Mech. 234 (2023) 2087–2101, http://dx.doi.org/10.1007/s00707-023-03485-7.

[17] J.C.H. Affdl, J.L. Kardos, The Halpin-Tsai equations: A review, Polym. Eng. Sci. 16 (5) (1976) 344–352, http://dx.doi.org/10.1002/pen.760160512.

[18] A. Ghorbanpour Arani, H. Baba Akbar Zarei, E. Haghparast, Application of halpin-tsai method in modelling and size-dependent vibration analysis of CNTs/fiber/polymer composite microplates., J. Comput. Appl. Mech. 47 (1) (2016) 45–52, http://dx.doi.org/10.22059/jcamech.2016.59254.

[19] Y. Zare, Development of Halpin-Tsai model for polymer nanocomposites assuming interphase properties and nanofiller size, Polym. Test. 51 (2016) 69–73, http://dx.doi.org/10.1016/j.polymertesting.2016.02.010.

[20] R. McCullough, Generalized combining rules for predicting transport properties of composite materials, Compos. Sci. Technol. 22 (1) (1985) 3–21, http://dx.doi.org/10.1016/0266-3538(85)90087-9.

[21] G. Martínez-Ayuso, M.I. Friswell, S. Adhikari, H.H. Khodaparast, H. Berger, Homogenization of porous piezoelectric materials, Int. J. Solids Struct. 113–114 (2017) 218–229, http://dx.doi.org/10.1016/j.ijsolstr.2017.03.003.

[22] J. Adhikari, R. Kumar, S.C. Jain, Using modified Halpin Tsai based approach for electromechanical analysis of functionally graded graphene reinforced piezoelectric tile, Int. J. Mech. Mater. Des. 19 (2) (2023) 299–318, http://dx.doi.org/10.1007/s10999-022-09632-7.

[23] H. Brito-Santana, R. de Medeiros, R. Rodriguez-Ramos, V. Tita, Different interface models for calculating the effective properties in piezoelectric composite materials with imperfect fiber–matrix adhesion, Compos. Struct. 151 (2016) 70–80, http://dx.doi.org/10.1016/j.compstruct.2016.02.003.

[24] M.H. Malakooti, H.A. Sodano, Multi-inclusion modeling of multiphase piezoelectric composites, Compos. B 47 (2013) 181–189, http://dx.doi.org/10.1016/j.compositesb.2012.10.034.

[25] J. Longo, M.R. Silva, H. Brito-Santana, A.J. Ferreira, V. Tita, R. de Medeiros, Development of a numerical and analytical methodology for analyzing hybrid laminates with multi-oriented piezoelectric and structural layers, Compos. Struct. 349–350 (2024) 118506, http://dx.doi.org/10.1016/j.compstruct.2024.118506.

[26] A. Araújo, C.M. Soares, J. Herskovits, P. Pedersen, Estimation of piezoelastic and viscoelastic properties in laminated structures, Compos. Struct. 87 (2009) 168–174, http://dx.doi.org/10.1016/j.compstruct.2008.05.009.

[27] A. Naik, N. Abolfathi, G. Karami, M. Ziejewski, Micromechanical viscoelastic characterization of fibrous composites, J. Compos. Mater. 42 (2008) 1179–1204, http://dx.doi.org/10.1177/0021998308091221.

[28] L. Bouhala, S. Ozyigit, A. Laachachi, A. Makradi, Multiscale finite element procedure to predict the effective elastic properties of woven composites, Compos. Part C: Open Access 15 (2024) 100539, http://dx.doi.org/10.1016/j.jcomc.2024.100539.

[29] W. Tian, L. Qi, X. Chao, J. Liang, M. Fu, Periodic boundary condition and its numerical implementation algorithm for the evaluation of effective mechanical properties of the composites with complicated micro-structures, Compos. B 162 (2019) 1–10, http://dx.doi.org/10.1016/j.compositesb.2018.10.053.

[30] A. Bueschel, S. Klinkel, W. Wagner, A viscoelastic model for dielectric elastomers based on a continuum mechanical formulation and its finite element implementation, in: Y. Bar-Cohen, F. Carpi (Eds.), Electroactive Polymer Actuators and Devices (EAPAD) 2011, Vol. 7976, SPIE, 2011, p. 79761R, http://dx.doi.org/10.1117/12.880283.

[31] X. Wang, J. Gao, Y. Wang, J. Bai, Z. Zhao, C. Luo, Finite element analysis for linear viscoelastic materials considering time-dependent Poisson's ratio: Variable stiffness method, Appl. Sci. (Switzerland) 14 (2024) http://dx.doi.org/10.3390/app14083189.

[32] E. Sánchez-Palencia, Non-Homogeneous Media and Vibration Theory, Springer, 1980.

[33] A. Ramírez-Torres, S. Di Stefano, A. Grillo, R. Rodríguez-Ramos, J. Merodio, R. Penta, An asymptotic homogenization approach to the microstructural evolution of heterogeneous media, Int. J. Non-Linear Mech. 106 (2018) 245–257, http://dx.doi.org/10.1016/j.ijnonlinmec.2018.06.012.

[34] O. Cruz-González, D. Guinovart-Sanjuán, R. Rodríguez-Ramos, J. Bravo-Castillero, R. Guinovart-Díaz, J. Merodio, R. Penta, J.A. Otero, S. Dumont, F. Lebon, F. Sabina, An approach for modeling non-ageing linear viscoelastic composites with general periodicity, Compos. Struct. 223 (2019) 110927, http://dx.doi.org/10.1016/j.compstruct.2019.110927.

[35] R. Guinovart-Díaz, J. Bravo-Castillero, R. Rodríguez-Ramos, F. Sabina, R. Martínez-Rosado, Overall properties of piezocomposite materials 1–3, Mater. Lett. 48 (2001) 93–98, http://dx.doi.org/10.1016/S0167-577X(00)00285-8.

[36] R. Guinovart-Díaz, P. Yan, R. Rodríguez-Ramos, J. López-Realpozo, C. Jiang, J. Bravo-Castillero, F. Sabina, Effective properties of piezoelectric composites with parallelogram periodic cells, Internat. J. Engrg. Sci. 53 (2012) 58–66, http://dx.doi.org/10.1016/j.ijengsci.2011.12.009.

[37] J. Bravo-Castillero, R. Guinovart-Díaz, F.J. Sabina, R. Rodríguez-Ramos, Closed-form expressions for the effective coefficients of a fiber-reinforced composite with transversely isotropic constituents – II. Piezoelectric and square symmetry, Mech. Mater. 33 (2001) 237–248, http://dx.doi.org/10.1016/S0167-6636(00)00060-0.